Journal of Catalysis 401 (2021) 1–6

Contents lists available at ScienceDirect

Journal of Catalysis

journal homepage: www.elsevier.com/locate/jcat

Mapping the coke formation within a zeolite catalyst extrudate in space and time by *operando* computed X-ray diffraction tomography

David S. Wragg [a,*], Georgios N. Kalantzopoulos [a], Dimitrios K. Pappas [a], Irene Pinilla-Herrero [a], Daniel Rojo-Gama [a], Evgeniy Redekop [a], Marco Di Michiel [b], Pablo Beato [c], Lars F. Lundegaard [c,*], Stian Svelle [a,*]

[a] Center for Materials Science and Nanotechnology (SMN), Department of Chemistry, University of Oslo, P.O. Box 1033, Blindern, N-0315 Oslo, Norway
[b] ESRF-The European Synchrotron, 71 Avenue des Martyrs, 38000 Grenoble, France
[c] Haldor Topsøe A/S, Haldor Topsøes Allé 1, 2800 Kgs. Lyngby, Denmark

ARTICLE INFO

Article history:
Received 16 April 2021
Revised 28 June 2021
Accepted 1 July 2021
Available online 8 July 2021

Keywords:
Binder
Deactivation
Imaging
Methanol
Methanol-to-hydrocarbons

ABSTRACT

We have used *operando* X-ray diffraction computed tomography (XRD-CT) analysed by rigorous crystallographic methods to reveal the behaviour of a zeolite/alumina based catalyst extrudate in the methanol-to-hydrocarbon reaction under working conditions ($T_{reaction}$ = 440 °C; ambient total pressure; WHSV = 12 $g_{MeOH}\ g^{-1}_{extrudate}\ h^{-1}$). By doing so, we demonstrate that it is possible to precisely monitor how the cylindrical extrudate is deactivated during the process by gradual filling with coke from the outer surface towards the core. The *operando* data thus collected are simulated by a model taking both the reaction kinetics and the diffusion within the extrudate into account, and this analysis provides the tools required for future optimization of the degree of utilization of the catalyst. Both the operando experiment and post mortem XRD-CT of fully deactivated extrudates from a test reactor show clearly that the core of the catalyst body, around 1/3 of its volume, remains completely untouched by the reaction, even when the reactor output indicates zero activity.

1. Introduction

Industrial catalysis is a critical enabling technology that is used to produce ca. 85–90% of all chemical products including transportation fuels, bulk and fine chemicals, as well as for pollution abatement [1]. When solid catalysts are employed in an industrial process, they are typically mixed with additives and binders (e.g. alumina) before being shaped into macroscopic objects such as extrudates, spheres, or pellets. The size of such shaped objects varies in the millimeter to centimeter range, depending on the mechanical strength, heat transfer characteristics, and other requirements of a specific process or reactor technology. In contrast, the vast majority of advanced investigations of the fundamental properties of catalysts, beyond straightforward measurements of activity, selectivity, and catalyst lifetime, are carried out using much simpler catalysts, i.e. powdered samples of the active component alone. While studies of the pure active components can help us to understand their intrinsic properties, the ultimate performance of catalysts in an industrial process can be strongly affected by the composition, morphology, and size of the composite macroscopic catalyst objects [2,3].

To gain a better understanding of the behaviour of a shaped catalyst extrudate in the methanol-to-hydrocarbons process, we have carried out a 5-dimensional time and space resolved *operando* X-ray diffraction computed tomography (XRD-CT) study. Space resolved studies of catalyst objects are rare in the literature, and mainly concern catalysts based on metallic or dense oxide catalysts which are strong scatterers of X-rays. Beale, Weckhuysen, and coworkers have applied XRD-CT to a range of metal/oxide catalyst systems [4,5], including operando studies [6–8] and have also developed pair distribution function analysis for this kind of data (PDF-CT) [9]. Other spatially resolved techniques which have been applied to catalyst bodies and particles include micro and nanotomography [10–14], fluorescence CT [15], scanning transmission X-ray microscopy [16–18] and nanobeam X-ray adsorption spectroscopy [19].

We have used *operando* XRD-CT to create an XRD-CT movie (see Supplementary Material) of the deactivation of a zeolite/alumina methanol to hydrocarbon (MTH) catalyst extrudate under working conditions with high time resolution (ca. 3.5 min per XRD-CT slice).

* Corresponding authors.
E-mail addresses: david.wragg@smn.uio.no (D.S. Wragg), lafl@topsoe.dk (L.F. Lundegaard), stian.svelle@kjemi.uio.no (S. Svelle).

https://doi.org/10.1016/j.jcat.2021.07.001
0021-9517/

The image series reveals the buildup of coke in both space and time using parameters from fully refined crystal structures with atomic resolution. We find that even when the extrudate is no longer catalytically active, a significant volume remains entirely free of coke, and we observe steep radial and axial gradients in coke content. Furthermore, we illustrate the power of *operando* XRD-CT to move beyond simple, strongly scattering metal and dense oxide materials.

MTH is an important process for the conversion of natural gas, coal, biogas, and even CO_2 into light alkenes that are used to produce polymers and transportation fuels [20]. We have previously demonstrated that it is possible to monitor the deactivation of the ZSM-5 zeolite by XRD [21,22]. Changes in certain parameters of the crystal structure of the ZSM-5 catalyst (the difference in length of the *a*- and *b*- unit cell vectors) are directly correlated to classic deactivation phenomena such as total coke content (from thermogravimetry), loss of acidity (from pyridine IR spectroscopy), reduction of surface area (from N_2 adsorption), as well as catalyst activity [21,22]. DFT has proved that bulky, non-reactive hydrocarbons are required to distort the unit cell in the manner observed [21]. Further, the residual electron as inferred from difference Fourier maps provides a second, independent measure of the concentration of coke compounds within the zeolite pores [21,22]. Here we use these well-established descriptors to study the coking in 5 dimensions (as defined by Beale et al. [23]: time, 3D space and chemical information).

2. Results

2.1. Operando XRD-CT

The bottom panel of Fig. 1 shows the mass spectrometry (MS) trace monitoring the MTH reaction using a single ZSM-5/alumina extrudate (cylinder, ca 1.6 × 6 mm) as the catalyst. Experimental detail is provided in the Supplementary Material. Clearly, there is stable and significant conversion for several hours before a gradual loss of activity occurs, as seen from the increase in the methanol and dimethyl ether intensities and corresponding decrease seen for the alkene products. These data confirm that the single extrudate acted as a highly active catalyst, and that a gradual reduction in the conversion occurred during the duration of the experiment (17 h on stream). This deactivation behavior is very similar to that observed in the home laboratory (see Supplementary Material).

The top panels of Fig. 1 show the evolution of the *a*-*b* parameter with increasing reaction time for three different slices of the extrudate. Note the upwards flow direction. We limited the investigation to three slices at the top middle and bottom of the extrudate to compromise between fast enough time resolution for a meaningful operando study and good enough spatial resolution within the slices to show the radial changes in detail. Quantitative Rietveld analysis of extrudates at different degrees of deactivation reveal that alumina and zeolite are evenly distributed within the extrudates (see Figure S.8 and Section 5 of the Supplementary Material). Thus, as the extrudate is quite homogeneous in composition and the entire object is exposed to the same reactant gas flow, we think it is reasonable to assume that the same axial trends seen in the 3 slices would be observed if more slices had been acquired. We will first focus first on radial gradients in the *a*-*b* descriptor (orange-black scale) keeping in mind the previously established link to key deactivation parameters such as coke content and loss of surface area and acidity [21,22]. It is evident from Fig. 1 that the change in the *a*-*b* parameter and thus the deactivation is initiated at or very near the outside of the extrudate followed by a slow, radial progress towards the center. The white-black circles of Fig. 1 shows the evolution of the degree of coking, as determined based on the residual electron density in the chan-

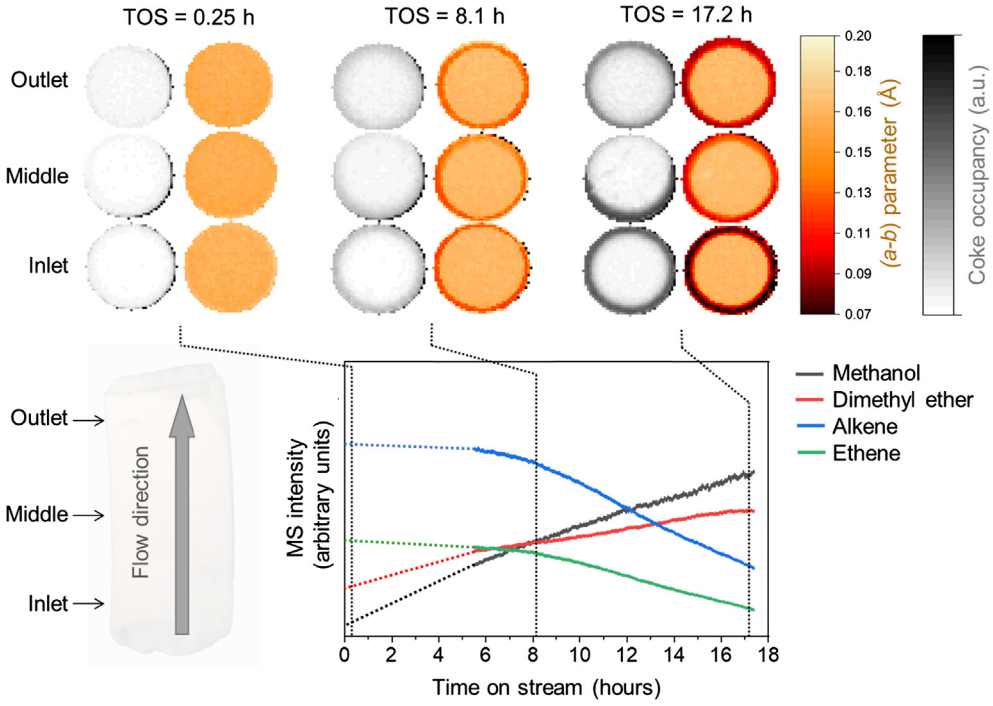

Fig. 1. Mapping the coke formation within a zeolite catalyst extrudate in space and time by *operando* computed X-ray diffraction tomography. Three horizontal slices of catalyst extrudate (1.6 × 6 mm) were scanned at different height/distance from reactor inlet (bottom left). Top: Tomograms showing the evolution in the *a*-*b* parameter (orange-black scale) and the degree of coking derived from the residual electron density (white-black scale) with increasing reaction time, respectively. Bottom: Mass spectrometry traces showing the catalyst activity and deactivation with increasing reaction time. Black = methanol, *m*/*z* 31; red = DME, *m*/*z* 45, green = ethene, *m*/*z* 28; blue = higher alkenes (C3 and above), *m*/*z* = 41. The first 5.5 h of data have been retrospectively extrapolated due to technical challenges with the MS during synchrotron experiment, and are consistent with similar experiments carried out in our catalyst test lab. The reaction conditions were WHSV = 12 $g_{MeOH}\ g^{-1}_{extrudate}\ h^{-1}$ and 440 °C. (For interpretation of the references to color in this figure legend, the reader is referred to the web version of this article.)

nels. The electron densities were quantified using a dummy atom method as described by Wragg et al. [24] (see Supplementary Material for further details). Both data analysis methods reveal the same radial evolution of the coking, again confirming the validity of the *a-b* parameter as a descriptor for catalyst deactivation. A similar core–shell type of coking was observed by Weckhuysen and co-workers in ex-situ experiments using fluorescent nanoprobes [25]. Turning finally to axial features, detailed analysis of the date behind Fig. 1 suggest that the coking does appear to be more profound near the reactor outlet (top). We attribute this to the fact that the MTH reaction is autocatalytic. Consequently, the hydrocarbon formation is initiated across a portion of the catalyst (bed or extrudate) at the inlet of the flow reactor. As coke formation necessarily occurs after the hydrocarbon formation, the coking is usually less severe at the reactor inlet [22,26–28].

2.2. Ex-situ/post morten XRD-CT

The time-resolved *operando* dataset from Fig. 1 does not cover the entire duration of catalyst deactivation, as is evident from the residual non-zero alkene production in the MS data (Fig. 1, bottom panel). Slow deactivation is one of the industrial advantages of ZSM-5 catalysts, but problematic for synchrotron experiments with a limited timeframe. To establish the final coke distribution, we collected *ex situ* XRD-CT on a completely deactivated catalyst extrudate. The sample was prepared in a fixed bed reactor in the home laboratory (see Supplementary Material). Fig. 2 shows the *a-b* parameter and the total coke occupancy for this fully-deactivated extrudate. These data were recorded with higher spatial resolution than the *operando* experiment, on an extrudate that was mounted horizontally. As there are no angular gradients (Fig. 1), this allows us to map the entire extrudate with a single XRD-CT scan. The maps confirm that at these conditions, a considerable interior portion of the extrudate (roughly 1/3 of the volume) remains coke-free when fully deactivated, i.e. the catalyst available is not fully utilized.

2.3. Analysis and simulations

We have demonstrated that the deactivation progresses radially from the outside towards the center of the extrudate. Therefore, the 4D (Cartesian space and time) dataset can be averaged around the central angle of each circular slice to reduce data dimensionality and increase the signal-to-noise ratio. Angle-averaged, 2D (radial coordinate and time) data for the top-most extrudate slice are presented in Fig. 3. The radial positions (r) are normalized against the radius of the pellet (R). The entire *operando* dataset for this slice is shown on the top left as a heat map in which the color intensity corresponds to the relative coke content (θ_{coke}). This is defined as the difference in the *a-b* parameter at a given time (t) and radial position (r) normalized to the maximum difference found for the fully deactivated extrudate:

$$\theta_{coke} = \frac{(a-b)_{fresh} - (a-b)_{t,r}}{(a-b)_{fresh} - (a-b)_{deact}}$$

These radial coking profiles, after filtering and normalization (see Supplementary Material), are shown in Fig. 3 (top right) at different time points during the experiment along with the radial profile of the completely (*ex-situ*) deactivated extrudate.

Data reduction and filtering reveals several new features not readily discerned in the individual 3D tomograms (Fig. 1). First, a continued build-up of coke occurs at the outer zone of the extrudate during the entire observation time, as evidenced by the raising plateau near the outer surface (vertical yellow arrow in top right panel). Second, the comparison of the *operando* dataset (colored) with the coke profile of the fully deactivated sample (shown in the same panel in black) reveals the extent of (incomplete) deactivation that we were able to capture within the limited timeframe of the *operando* experiment (17 h). Finally, the spatio-temporal kinetics of coking exhibit an initiation period of relatively slow growth (yellow arrow in top left panel), followed by a rapid acceleration and an eventual slow-down towards an asymptotic value.

These features are emphasized in three panels at the bottom of Fig. 3, which depict the time evolution of three metrics constructed from the dataset. The bottom left panel shows the normalized coke content in the plateau region near the outer surface; the bottom middle panel shows the radial position of the coking front, as defined by the radial position at which the normalized coke content exceeds 0.05 (5%), and the bottom right panel shows the fraction of the catalyst extrudate that remains free of coke, defined as one minus the area under each normalized coke profile in the top right panel of Fig. 3 (1-f_{coke}). This behavior is reminiscent of a well-known auto-catalytic character of the MTH reaction [20], which was also observed for the axial progression of coke deposition along a packed bed of pelletized (non-extruded) zeolite [22,28]. Unlike these previous studies, in which no intra-particle coke gradients were resolved, our data reveal autocatalytic coking at the *meso*-scale within a single catalyst extrudate.

We constructed a simple transient 1D reaction/diffusion model to capture the initiation period and the eventual asymptotic slowing of coke deposition (see details of the model in Supplementary Material). Simulated spatio-temporal coke profiles are depicted in Fig. 4. With manually adjusted parameters, the model adequately reproduces the general features of the experimental dataset such as a delay in coke formation during the initiation period, the time-scale of the coking front propagation, and the eventual asymptotic saturation of the catalyst with coke. It should be noted that the simulated coking front appears sharper in both, space and time in comparison with the experimental data in Fig. 4, since our

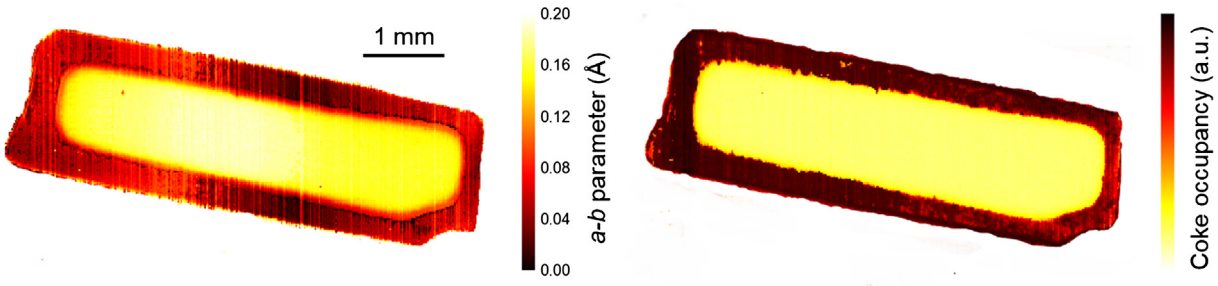

Fig. 2. XRD-CT slices through a horizontally mounted extrudate. Left: The *a-b* parameter (Å) for a severely deactivated extrudate. Right: The degree of coking from the residual electron density (arbitrary units). ZSM-5/alumina extrudates were deactivated *ex situ* at WHSV = 12 $g_{MeOH}\ g^{-1}_{extrudate}\ h^{-1}$ and 400 °C prior to XRD-CT analysis.

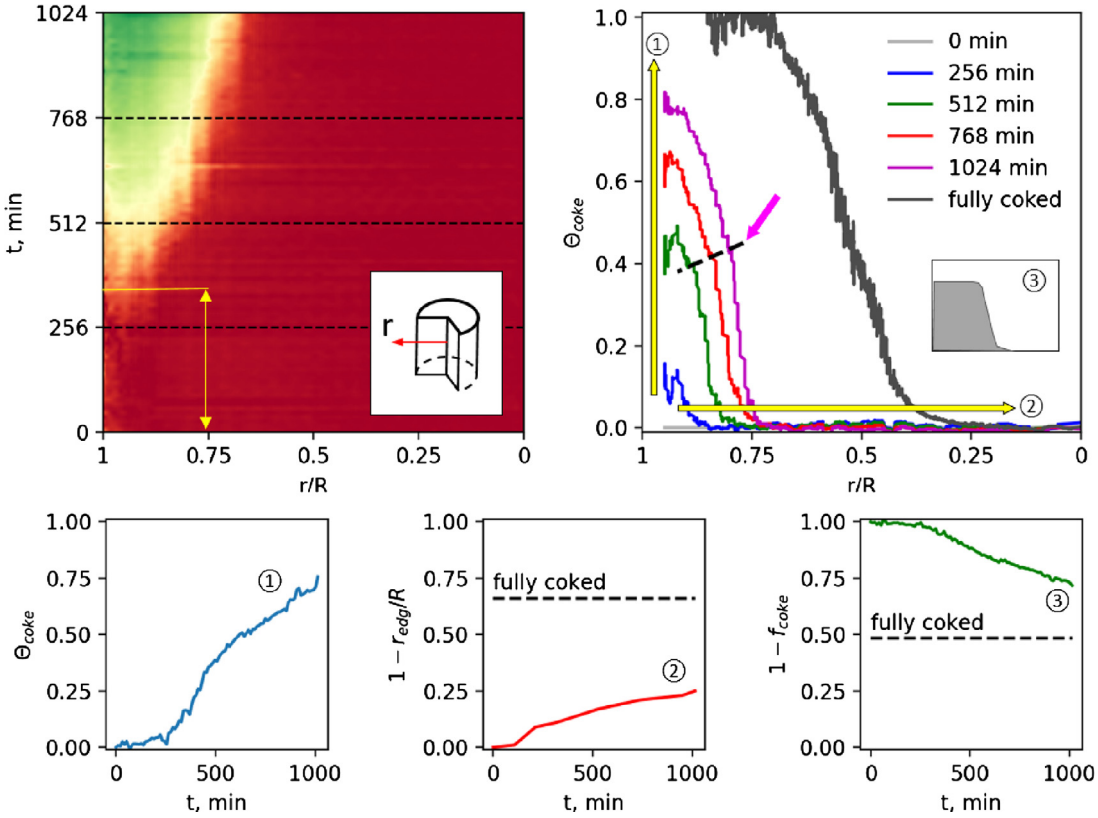

Fig. 3. Evolution of angle-averaged radial coke profiles from XRD-CT. Data are shown for the topmost slice of the catalyst extrudate. Top left: An overview of the angle-averaged coke content as a function of normalized radial coordinate (x-axis, r/R) and time (y-axis, t). The color map is scaled from the lowest coke content (orange) to the highest (green), with the yellow arrow indicating the delay in coke formation. The inset depicts the definition of the angle-averaged radial coordinate (r = 0 at the extrudate center). Top right: Radial coke profiles at selected time points (indicated as black dashed lines on the left) along with the profile for a fully coked extrudate (black). Yellow arrows are shown to guide the eye in the directions of coke growth, while the pink arrow points to the highly non-linear features of the coking profile (slope change). Bottom panels: Temporal evolution of coke content in the catalytic extrudate. Bottom left: Relative coke content within the outermost extrudate shell (see vertical arrow in the top right panel). Bottom middle: Relative radial position of the coking front (see horizontal arrow in the top right panel). Bottom right: Relative coke-free fractional volume of the catalyst extrudate. All data are normalized to the maximal amount of coke in the fully deactivated extrudate. (For interpretation of the references to color in this figure legend, the reader is referred to the web version of this article.)

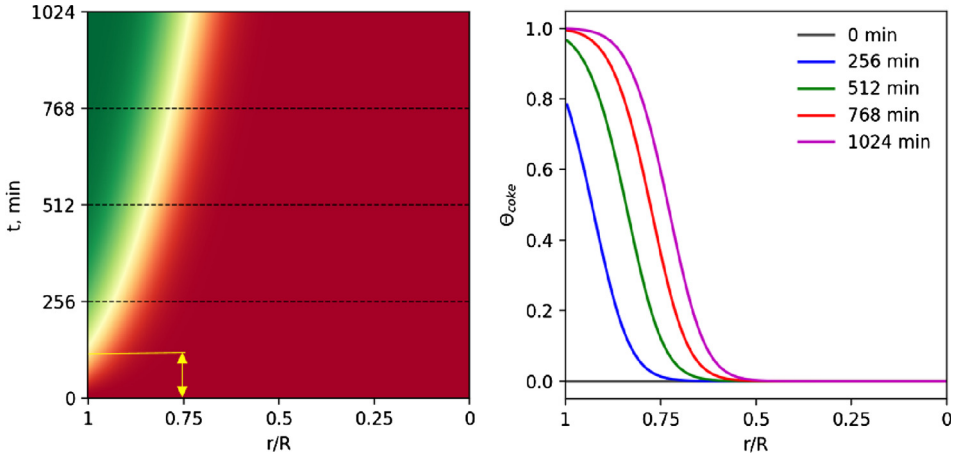

Fig. 4. Simulated radial coke profiles qualitatively recreating the salient features of the experimental data presented in Fig. 3. Left: An overview of the angle-averaged coke content as a function of normalized radial coordinate (x-axis, r/R) and time (y-axis, t). The color map is scaled from the lowest coke content (orange) to the highest (green), with the yellow arrow indicating the delay in coke formation. Right: Radial coke profiles at selected time points (indicated as black dashed lines on the left panel). (For interpretation of the references to color in this figure legend, the reader is referred to the web version of this article.)

model did not contain high-frequency noise. Importantly, although not in full quantitative agreement with experimental data (e.g. shorter delay in coke formation), the model correctly predicts that the inner core of the extrudate remains free of coke due to mass-transfer limited methanol conversion.

3. Discussion

The reported findings have major implications for the catalytic technology in terms of optimizing the efficiency of catalyst utilization. It is evident from Fig. 2 that even for a severely deactivated

extrudate, the deactivation occurs only within its outer shell. Importantly, XRD-CT reconstructions using the weight percentage of the two components of the extrudate show that the zeolite catalyst and the alumina binder are evenly distributed (Supplementary Material, Figure S.8). Our analysis reveals that, for the extrudate in Fig. 2, around 1/3 of the catalyst volume has not been exposed to methanol. It should be emphasized that a high space velocity and reaction temperature (WHSV = 12 g_{MeOH} $g^{-1}_{extrudate}$ h^{-1} and 440 °C) was employed to shorten the experiment time to make it suitable for synchrotron studies. We anticipate that the fraction of the catalyst extrudate exposed to methanol will be greater at lower feed rates. Further, the size and porosity of the shaped catalyst object requires attention. Weckhuysen and co-workers have observed quite similar core–shell features in the coking of several MTH catalyst extrudates of different size using staining and confocal microscopy [25]. This was attributed to a stepwise narrowing of the porosity of the extrudates from surface to center. However, for sufficiently small extrudates, no transport limitations were detected and consequently a full utilization of the extrudate was found [25]. The same team studied the effects of the type of binder using and UV–Vis spectroscopy for aromatics transalkylation and again observed core–shell deactivation behavior. Further, a profound effect of the choice of binder material on the properties of the catalyst extrudate was found, as a much greater accessibility for bulky probe molecules was seen when alumina was used rather than silica [29,30]. Invariably, it becomes clear that the shaping, which is an absolute requirement for industrial use of a zeolite catalyst, might lead to an inefficient use of the catalyst. Indeed, an analysis presented by Rao and Coppens suggests that optimization of the porosity of a shaped hydrodemetallation catalyst can lead to a 21% reduction of the amount of catalyst material required [31]. Clearly, efforts to balance the effects of both reaction conditions and the catalyst properties on the efficiency of the catalyst utilization is a topic for further studies.

The primary strength in our approach, however, lies in the possibility of being able to monitor the coking continuously with resolution in time and space (*operando*), which enables quantitative comparison of experimental observations with numerical simulations, eventually using real kinetic and spatial models based on chemically meaningful parameters. These possibilities motivate further developments of the XRD-CT methodology with the aim of maximizing the signal-to-noise ratio, while maintaining excellent time resolution. Acquiring such data in real time (i.e. operando) with spatio-temporal resolution and chemical specificity is likely to provide valuable input to the parametrization of multiscale chemical reaction engineering models [32] of MTH processes [33]. We foresee that as the barrier to performing the experiments and carrying out detailed crystallographic analysis of every voxel falls lower, XRD-CT will find many new users. New instruments and methods are opening up possibilities for studying tiny particles with high spatial resolution [34] and larger objects [35], which would previously have been impossible to reconstruct without blurring. Clearly, XRD-CT is a powerful operando technique to obtain time and space resolved information that, especially when coupled with ex-situ characterization and modeling, can provide new fundamental insights into complex chemical phenomena.

4. Conclusion

In conclusion, we have employed *operando* computed X-ray diffraction tomography to monitor the deactivation of shaped zeolite catalyst extrudates, comprising both the active zeolite component and alumina binder, in time (time on stream) and space (the volume of the extrudate; 6 mm long by 1.6 mm diameter). We demonstrate that during the conversion of methanol to hydrocarbons, the deactivation starts at the external part of the extrudate and progresses radially inwards. By carrying out *operando* XRD-CT, we are able to track the deactivation in time and space and to couple these observations to a simple, yet chemically meaningful kinetic model. These simulations uncovered hitherto undescribed non-linear features of the coking kinetics. Clearly, *operando* observation coupled with modelling will pave the way for improved catalyst and process design. Indeed, by extending the study to include ex situ characterization of severely deactivated extrudates, we show, in line with previous reports, that only a certain fraction of the catalyst is exposed to feedstock and employed in the catalytic process. Our observations might thus lead to substantial process intensification and savings in terms of more efficient catalyst utilization and/or smaller chemical reactors by optimization of reaction conditions and the extrudate properties. Finally, our work is the first demonstration of *operando* XRD-CT for low-scattering, non-transition metal containing catalysts. In contrast to most previous work, we have carried out a full parametric Rietveld refinement for the datasets in every voxel and evaluated the data against a kinetic reaction–diffusion model. The methodological breakthroughs presented herein will lead to significant improvements of our understanding of zeolite catalysts and deactivation phenomena with great technological impact.

5. Methods

Operando XRD-CT was collected at the ID15A beamline at the European Synchrotron (ESRF). The catalyst, a single alumina/ZSM-5 extrudate of size 1.6 × 6 mm, was placed in a vertical quartz tube (2 mm ID) held in a custom built furnace with an opening for the X-ray beam. The reaction conditions were WHSV = 12 g_{MeOH} $g^{-1}_{extrudate}$ h^{-1} and 440 °C and the total duration of the experiment was ∼ 17 h. Full experimental details are provided in the Supplementary Material.

Declaration of Competing Interest

The authors declare that they have no known competing financial interests or personal relationships that could have appeared to influence the work reported in this paper.

Acknowledgements

The authors acknowledge ESRF for granting beamtime at ID15A. This work is partially funded by the European Industrial Doctorate Project “ZeoMorph” (Grant Agreement No. 606965), the Innovation Fund Denmark (Ref. 5190-00019B), and the Research Council of Norway via the iCSI Centre for Research-based Innovation (contract no. 237922) and the TomoCAT researcher project (project no. 301619).

Appendix A. Supplementary material

Supplementary data to this article can be found online at https://doi.org/10.1016/j.jcat.2021.07.001.

References

[1] P. Lanzafame, S. Perathoner, G. Centi, S. Gross, E.J.M. Hensen, Grand challenges for catalysis in the science and technology roadmap on catalysis for Europe: moving ahead for a sustainable future, Catal. Sci. Technol. 7 (2017) 5182–5194.
[2] G.T. Whiting, S.H. Chung, D. Stosic, A.D. Chowdhury, L.I. van der Wal, D.L. Fu, J. Zecevic, A. Travert, K. Houben, M. Baldus, B.M. Weckhuysen, Multiscale mechanistic insights of shaped catalyst body formulations and their impact on catalytic properties, ACS Catal. 9 (2019) 4792–4803.
[3] N.L. Michels, S. Mitchell, J. Perez-Ramirez, Effects of binders on the performance of shaped hierarchical MFI zeolites in methanol-to-hydrocarbons, ACS Catal. 4 (2014) 2409–2417.

[4] A.M. Beale, E.K. Gibson, M.G. O'Brien, S.D.M. Jacques, R.J. Cernik, M. Di Michiel, P.D. Cobden, O. Pirgon-Galin, L. van de Water, M.J. Watson, B.M. Weckhuysen, Chemical imaging of the sulfur-induced deactivation of Cu/ZnO catalyst bodies, J Catal 314 (2014) 94–100.
[5] C.K. Egan, S.D.M. Jacques, M.D. Wilson, M.C. Veale, P. Seller, A.M. Beale, R.A.D. Pattrick, P.J. Withers, R.J. Cernik, 3D chemical imaging in the laboratory by hyperspectral X-ray computed tomography, Sci Rep-Uk 5 (2015).
[6] M.G. O'Brien, S.D.M. Jacques, M. Di Michiel, P. Barnes, B.M. Weckhuysen, A.M. Beale, Active phase evolution in single Ni/Al2O3 methanation catalyst bodies studied in real time using combined mu-XRD-CT and mu-absorption-CT, Chem Sci 3 (2012) 509–523.
[7] S.D.M. Jacques, M. Di Michiel, A.M. Beale, T. Sochi, M.G. O'Brien, L. Espinosa-Alonso, B.M. Weckhuysen, P. Barnes, Dynamic X-ray diffraction computed tomography reveals real-time insight into catalyst active phase evolution, Angew Chem Int Edit 50 (2011) 10148–10152.
[8] L. Espinosa-Alonso, M.G. O'Brien, S.D.M. Jacques, A.M. Beale, K.P. de Jong, P. Barnes, B.M. Weckhuysen, Tomographic energy dispersive diffraction imaging to study the genesis of Ni nanoparticles in 3D within gamma-Al_2O_3 catalyst bodies, J Am Chem Soc 131 (2009) 16932–16938.
[9] S.D.M. Jacques, M. Di Michiel, S.A.J. Kimber, X.H. Yang, R.J. Cernik, A.M. Beale, S. J.L. Billinge, Pair distribution function computed tomography, Nat Commun 4 (2013).
[10] D. Matras, S.D.M. Jacques, H.R. Godini, M. Khadivi, J. Drnec, A. Poulain, R.J. Cernik, A.M. Beale, Real-time operando diffraction imaging of La-Sr/CaO during the oxidative coupling of methane, J Phys Chem C 122 (2018) 2221–2230.
[11] D. Matras, S.D.M. Jacques, S. Poulston, N. Grosjean, C.E. Bosch, B. Rollins, J. Wright, M. Di Michiel, A. Vamvakeros, R.J. Cernik, A.M. Beale, Operando and postreaction diffraction imaging of the La-Sr/CaO catalyst in the oxidative coupling of methane reaction, J Phys Chem C 123 (2019) 1751–1760.
[12] A.M. Beale, S.D.M. Jacques, M. Di Michiel, J.F.W. Mosselmans, S.W.T. Price, P. Senecal, A. Vamvakeros, J. Paterson, X-ray physico-chemical imaging during activation of cobalt-based Fischer-Tropsch synthesis catalysts, Philos T R Soc A 376 (2018).
[13] A. Vamvakeros, S.D.M. Jacques, M. Di Michiel, D. Matras, V. Middelkoop, I.Z. Ismagilov, E.V. Matus, V.V. Kuznetsov, J. Drnec, P. Senecal, A.M. Beale, 5D operando tomographic diffraction imaging of a catalyst bed, Nat Commun 9 (2018).
[14] A.M. Beale, S.D.M. Jacques, B.M. Weckhuysen, Chemical imaging of catalytic solids with synchrotron radiation, Chem Soc Rev 39 (2010) 4656–4672.
[15] S.W.T. Price, D.J. Martin, A.D. Parsons, W.A. Slawinski, A. Vamvakeros, S.J. Keylock, A.M. Beale, J.F.W. Mosselmans, Chemical imaging of Fischer-Tropsch catalysts under operating conditions, Sci Adv 3 (2017).
[16] S. Kalirai, P.P. Paalanen, J. Wang, F. Meirer, B.M. Weckhuysen, Visualizing dealumination of a single zeolite domain in a real-life catalytic cracking particle, Angew Chem Int Edit 55 (2016) 11134–11138.
[17] L.R. Aramburo, J. Ruiz-Martinez, L. Sommer, B. Arstad, R. Buitrago-Sierra, A. Sepulveda-Escribano, H.W. Zandbergen, U. Olsbye, F.M.F. de Groot, B.M. Weckhuysen, X-Ray imaging of SAPO-34 molecular sieves at the nanoscale: influence of steaming on the methanol-to-hydrocarbons reaction, ChemCatChem 5 (2013) 1386–1394.
[18] L.R. Aramburo, E. de Smit, B. Arstad, M.M. van Schooneveld, L. Sommer, A. Juhin, T. Yokosawa, H.W. Zandbergen, U. Olsbye, F.M.F. de Groot, B.M. Weckhuysen, X-ray imaging of zeolite particles at the nanoscale: influence of steaming on the state of aluminum and the methanol-to-olefin reaction, Angew Chem Int Edit 51 (2012) 3616–3619.
[19] D.J. Martin, D. Decarolis, R. Tucoulou, G. Martinez-Criado, A.M. Beale, Towards the interrogation of the behaviour of a single nanoparticle under realistic catalytic reaction conditions, Catal Struct React 3 (2017) 63–70.
[20] U. Olsbye, S. Svelle, M. Bjorgen, P. Beato, T.V.W. Janssens, F. Joensen, S. Bordiga, K.P. Lillerud, Conversion of methanol to hydrocarbons: how zeolite cavity and pore size controls product selectivity, Angew Chem Int Edit 51 (2012) 5810–5831.
[21] D. Rojo-Gama, M. Nielsen, D.S. Wragg, M. Dyballa, J. Holzinger, H. Falsig, L.F. Lundegaard, P. Beato, R.Y. Brogaard, K.P. Lillerud, U. Olsbye, S. Svelle, A straightforward descriptor for the deactivation of zeolite catalyst H-ZSM-5, ACS Catal. 7 (2017) 8235–8246.
[22] D. Rojo-Gama, L. Mentel, G.N. Kalantzopoulos, D.K. Pappas, I. Dovgaliuk, U. Olsbye, K.P. Lillerud, P. Beato, L.F. Lundegaard, D.S. Wragg, S. Svelle, Deactivation of zeolite catalyst H-ZSM-5 during conversion of methanol to gasoline: operando time- and space-resolved X-ray diffraction, J Phys Chem Lett 9 (2018) 1324–1328.
[23] A.M. Beale, S.D.M. Jacques, E.K. Gibson, M. Di Michiel, Progress towards five dimensional diffraction imaging of functional materials under process conditions, Coordin Chem Rev 277 (2014) 208–223.
[24] D.S. Wragg, D. Akporiaye, H. Fjellvag, Direct observation of catalyst behaviour under real working conditions with X-ray diffraction: comparing SAPO-18 and SAPO-34 methanol to olefin catalysts, J Catal 279 (2011) 397–402.
[25] G.T. Whiting, N. Nikolopoulos, I. Nikolopoulos, A.D. Chowdhury, B.M. Weckhuysen, Visualizing pore architecture and molecular transport boundaries in catalyst bodies with fluorescent nanoprobes, Nat Chem 11 (2019) 23–31.
[26] J.F. Haw, D.M. Marcus, Well-defined (supra)molecular structures in zeolite methanol-to-olefin catalysis, Top Catal 34 (2005) 41–48.
[27] H. Schulz, "Coking" of zeolites during methanol conversion: Basic reactions of the MTO- MTP- and MTG processes, Catal Today 154 (2010) 183–194.
[28] D. Rojo-Gama, S. Etemadi, E. Kirby, K.P. Lillerud, P. Beato, S. Svelle, U. Olsbye, Time- and space-resolved study of the methanol to hydrocarbons (MTH) reaction - influence of zeolite topology on axial deactivation patterns, Faraday Discuss 197 (2017) 421–446.
[29] S.P. Verkleij, G.T. Whiting, D. Pieper, S.P. Esclapez, S.W. Li, M.M. Mertens, M. Janssen, A.J. Bons, M. Burgers, B.M. Weckhuysen, Chemical imaging of the binder-dependent coke formation in zeolite-based catalyst bodies during the transalkylation of aromatics, ChemCatChem 11 (2019) 4788–4796.
[30] S.P. Verkleij, G.T. Whiting, E.S. Parres, S.W. Li, M.M. Mertens, M. Janssen, A.J. Bons, M. Burgers, B.M. Weckhuysen, High-pressure operando UV-Vis micro-spectroscopy of coke formation in zeolite-based catalyst extrudates during the transalkylation of aromatics, ChemCatChem 12 (2020) 5465–5475.
[31] S.M. Rao, M.O. Coppens, Mitigating deactivation effects through rational design of hierarchically structured catalysts: application to hydrodemetalation, Ind. Eng. Chem. Res. 49 (2010) 11087–11097.
[32] F.J. Keil, Molecular modelling for reactor design, Annu Rev Chem Biomol 9 (2018) 201–227.
[33] M. Ye, H. Li, Y. Zhao, T. Zhang, Z. Liu, Chapter five - MTO processes development: the key of mesoscale studies, Adv. Chem. Eng. 47 (2015) 279–335.
[34] D.P. Finegan, A. Vamvakeros, C. Tan, T.M.M. Heenan, S.R. Daemi, N. Seitzman, M. Di Michiel, S. Jacques, A.M. Beale, D.J.L. Brett, P.R. Shearing, K. Smith, Spatial quantification of dynamic inter and intra particle crystallographic heterogeneities within lithium ion electrodes, Nat. Commun. 11 (2020).
[35] A. Vamvakeros, A.A. Coelho, D. Matras, H. Dong, Y. Odarchenko, S.W.T. Price, K. T. Butler, O. Gutowski, A.C. Dippel, M. Zimmermann, I. Martens, J. Drnec, A.M. Beale, S.D.M. Jacques, DLSR: a solution to the parallax artefact in X-ray diffraction computed tomography data, J. Appl. Crystallogr. 53 (2020) 1531–1541.